

Climate Mechanism for Stronger Typhoons in a Warmer World*

NAM-YOUNG KANG

National Typhoon Center/Korea Meteorological Administration, Jeju, South Korea

JAMES B. ELSNER

Department of Geography, and Geophysical Fluid Dynamics Institute, Florida State University, Tallahassee, Florida

(Manuscript received 19 August 2015, in final form 18 November 2015)

ABSTRACT

Violent typhoons continue to have catastrophic impacts on economies and welfare, but how they are responding to global warming has yet to be fully understood. Here, an empirical framework is used to explain physically why observations support a tight connection between increasing ocean warmth and the increasing intensity of supertyphoons in the western North Pacific. It is shown that the energy needed for deep convection is on the rise with greater heat and moisture in the lower tropical troposphere but that this energy remains untapped when air pressure is high. Accordingly, tropical cyclone formation is becoming less common, but those that do form are likely to reach extreme intensities from the discharge of stored energy. These thermodynamic changes to the environment most significantly influence the upper portion of extreme typhoon intensities, indicating that supertyphoons are likely to be stronger at the expense of overall tropical cyclone occurrences in the western North Pacific.

1. Introduction

The changing nature of tropical cyclone (TC) climate is an important concern in relation to anthropogenic global warming. In particular, the western North Pacific accounts for about one-third of all TCs worldwide (Chan 2005). The recent onslaught of supertyphoons makes countries tense from anticipation about future TC activity. Supertyphoon Haiyan in 2013 struck the Philippines, destroyed more than a million houses, and killed 6300 people [National Disaster Risk Reduction and Management Council (NDRRMC 2014)]. Even Supertyphoons Vongfong and Hagupit in 2014 rapidly developed into typhoons with intensities comparable to Haiyan. Over a million people were evacuated in the Philippines with the threat of Supertyphoon Hagupit.

People may suspect that global warming has a connection with TCs becoming violent in this ocean basin. Trends in annual TC occurrence rates have been investigated (Webster et al. 2005), but the influence of global warming is difficult to detect against the background of natural variation (Chan 2006, 2008). Additionally, observed trends can result simply from improvements in the quality of observations (Kossin et al. 2013), and estimated trends depend on the range of years considered (Klotzbach 2006). A long period of record is preferable, but there is no guarantee of reduced uncertainty. For these reasons, TC climate studies have tended toward a reliance on numerical model simulations (Knutson et al. 2010). Yet results from these studies remain inconclusive (IPCC 2013).

Here we provide a physical explanation for how extreme TCs in the western North Pacific respond to global warming and to their large-scale environments. New understanding is made possible by using an empirical framework with a consistent set of reliable observations (Kang and Elsner 2012a,b). The framework is motivated by the link between TC frequency and intensity (Emanuel 2008; Elsner et al. 2008). By projecting global ocean temperature variation onto a two-dimensional continuous frequency–intensity space (Kang and Elsner 2015), we

 Denotes Open Access content.

*Florida State University Contribution Number 475.

Corresponding author address: Nam-Young Kang, 2 Seosung 810-gil, Namwon, Seogwipo, Jeju 699-942, South Korea.
E-mail: nkang.fsu@gmail.com

DOI: 10.1175/JCLI-D-15-0585.1

are able to give an integrated assessment of typhoon climate. Section 2 describes the data and framework. Section 3 shows the statistical results, and section 4 explains them physically. Section 5 describes the connection between supertyphoons and global ocean warmth. Section 6 provides a summary of the results and a discussion. All the statistics and figures are created using R software (www.r-project.org) and are available online (<http://rpubs.com/Namyong/P2015a>).

2. Methodology

a. Data

We first organize a set of TC best tracks from the U.S. Joint Typhoon Warning Center (JTWC; www.usno.navy.mil/NOOC/nmfc-ph/RSS/jtwc/best_tracks) and the Japan Meteorological Agency (JMA; www.jma.go.jp/jma/jma-eng/jma-center/rsmc-hp-pub-eg/trackarchives.html). More than one TC dataset is available in the western North Pacific. Different observation procedures by different operational agencies create inconsistencies in the values within the dataset over time. For example, prior studies have tried to find a consensus among the estimated TC intensities from the various agencies (Song et al. 2010; Knapp and Kruk 2010) by matching individual TC events. But this turns out to be a difficult task.

Another problem is that analysis results using a particular dataset tend to vary according to the period of data used. A long period is preferred to minimize statistical uncertainty, but this comes at the expense of uneven data quality. A compromise is a selection of a useful period that contains as many reliable observations as possible. The longest period of reliable western North Pacific TC data is one that extends back to 1984 (Kang and Elsner 2012b). The data consist of lifetime-maximum winds (LMWs) from TCs during June through November (JJASON) over the 30-yr period 1984–2013. Other environmental variables, such as sea surface temperature (SST), Southern Oscillation index (SOI), air temperature, specific humidity, and geopotential height come from the National Oceanic and Atmospheric Administration (NOAA)/National Centers for Environmental Prediction (NCEP) reanalysis (www.esrl.noaa.gov/psd/data/gridded). Specifically, we utilize monthly SSTs from the Extended Reconstructed Sea Surface Temperature (ERSST), version 3b. SOI comes from the NOAA/Climate Prediction Center (CPC; www.cpc.ncep.noaa.gov/data/indices/soi).

b. Framework

To investigate TC climate variability, we first define equally contributing indicators. A schematic diagram

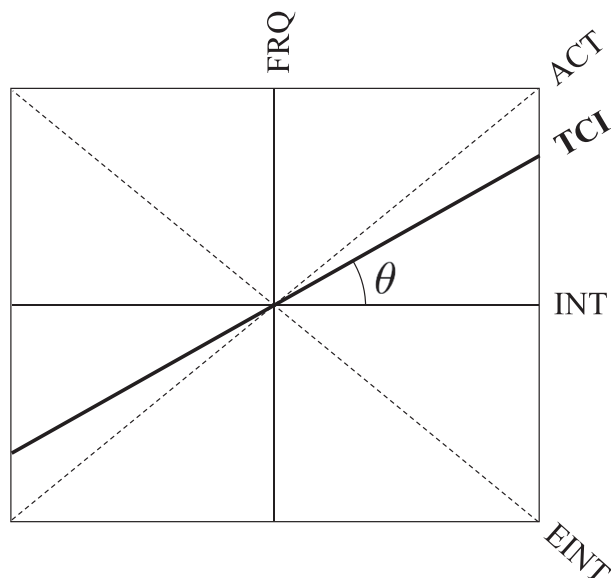


FIG. 1. Schematic of our TC climate framework. The positive diagonal (positive slope) captures the level of coherence between **FRQ** and **INT**. The negative diagonal (negative slope) captures the level of discordance. The state of the TC climate can be represented as a single point in the two-dimensional variability space. A variability direction of TC climate is shown as a thick black line. The angle starting from **INT** is θ . **ACT** and **EINT** are the special cases when θ is $+45^\circ$ and -45° , respectively. **ACT** and **EINT** are formed by equal weighting of **INT** and **FRQ**.

for our framework Kang and Elsner (2012a,b) is shown in Fig. 1. **INT** is the annual mean intensity of TCs having LMWs exceeding a threshold quantile. The lowest threshold quantile (zero empirical probability level—probability of a TC having weaker winds) is set as 17 ms^{-1} . **INT** can be computed at successively higher thresholds. **FRQ** is the annual number of TCs above each successive threshold. By definition, the variation of **FRQ** is not affected by the probability level. For example, the **FRQ** variation of the 50% strongest portion of TCs is the same as that of the total TCs. **INT** is on the horizontal axis, and **FRQ** is on the vertical axis.

An annual value in the upper-right quadrant represents high values of **INT** and **FRQ**, while an annual value in the lower-left quadrant represents low values of **INT** and **FRQ**. Thus, a positive diagonal line provides an axis that captures the in-phase relationship between **INT** and **FRQ** that we denote as **ACT**. **ACT** can be obtained by principal component analysis and is computed as

$$\mathbf{ACT} = \left(\frac{\mathbf{INT} - \mu_{\mathbf{INT}}}{\sigma_{\mathbf{INT}}} + \frac{\mathbf{FRQ} - \mu_{\mathbf{FRQ}}}{\sigma_{\mathbf{FRQ}}} \right) / \sqrt{2}, \quad (1)$$

where **INT** and **FRQ** are vectors of annual values, and μ and σ denote their respective mean and standard

deviations. **ACT** indicates the in-phase relationship between **INT** and **FRQ**, which is comparable to TC energy as indicated by its high correlation (Kang and Elsner 2012a) with accumulated cyclone energy (ACE; Bell et al. 2000) and power dissipation index (PDI; Emanuel 2005). On the other hand, a value in the upper-left quadrant is characterized by low **INT** and high **FRQ**, and a value in the lower-right quadrant shows high **INT** and low **FRQ**. Thus, a negative diagonal line provides an axis that captures the out-of-phase relationship between **INT** and **FRQ**. This variability is denoted by **EINT** as the efficiency of intensity. Alternatively, the negative **EINT** can be understood as the efficiency of frequency. **EINT** is the other principal component and is computed as

$$\mathbf{EINT} = \left(\frac{\mathbf{INT} - \mu_{\mathbf{INT}}}{\sigma_{\mathbf{INT}}} - \frac{\mathbf{FRQ} - \mu_{\mathbf{FRQ}}}{\sigma_{\mathbf{FRQ}}} \right) / \sqrt{2}. \quad (2)$$

Owing to the presence of **EINT**, a continuous two-dimensional variability space is formed, where the center is the mean of each standardized set of **FRQ** and **INT** values. Now, an annual TC climate can be indicated by a single point in the continuous variability space. In this framework, variability in any direction can be defined as

$$\mathbf{TCI}_\theta = \mathbf{INT} \cos \theta + \mathbf{FRQ} \sin \theta, \quad (3)$$

where **TCI** denotes a directional variability θ away from **INT** (positive is counterclockwise), which represents the weighted linear combination of **FRQ** and **INT**. **ACT** and **EINT** are the special cases when θ is $+45^\circ$ and -45° , respectively.

3. Correlation screen

Figure 2 illustrates the empirical framework and the correlation circle for the strongest 10% (0.9 probability level—90% of the TCs have winds weaker than this) of western North Pacific TCs based on 30 years of JJASON observations. The average wind speed for this subset is 67 m s^{-1} using the JTWC dataset, which nearly matches the supertyphoons of category 5 on the Saffir–Simpson scale (Simpson 1974). The quantile method is useful for dealing with the intensity variation of fewer events (Elsner et al. 2008). With an increase in supertyphoon intensities, the threshold LMW of the strongest 10% of TCs increases above 67 m s^{-1} , and **INT** over the threshold increases. The average wind speed of the strongest 10% of TCs using the JMA dataset is 49 m s^{-1} . On the other hand, the variation in **FRQ** is not affected by the probability level by definition. The annual variation in the number

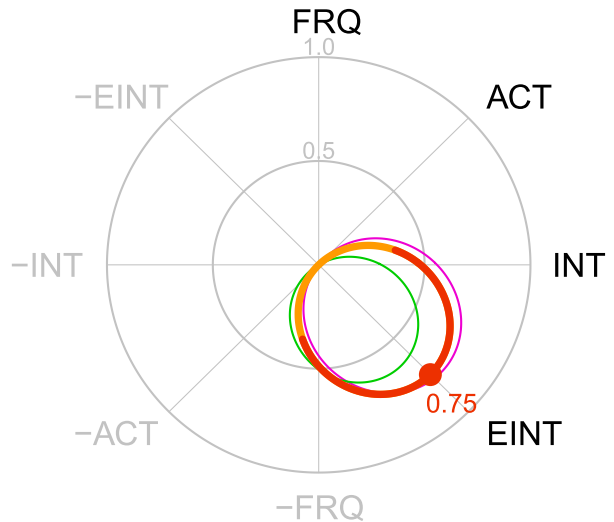


FIG. 2. Correlation screen of global ocean warmth and climate variability using the strongest 10% of all TCs in the western North Pacific. Global mean SST is used as global ocean warmth indicator. All indicators used for correlations are annual values averaged for JJASON over 30 years (1984–2013). The center, inner circle, and outer circle indicate the correlation levels of 0, 0.5, and 1, respectively. Correlations for JTWC and JMA are shown in purple and green loops, respectively. Each loop is a polygon linking 360 correlation values at 1° intervals. The orange line shows the correlation of global ocean warmth with composite TC climate from JTWC and JMA. The red portion of the line represents the significant ($\alpha \leq 0.05$) range of correlations. The dot indicates the direction of the largest correlation.

of all TCs should match the annual variation in the number of just the top 10% of them. Since this quantile approach controls **INT** only, the interpretation of the empirical framework centers on the relationship between overall TC occurrences and the intensity of the upper 10% subset.

Circular directions in Fig. 2 represent each TC climate variability, where **INT** and **FRQ** have different weights by an angle [see Eq. (3)]. Correlations are calculated for each directional variability of TC climate with global ocean warmth (indicated by global mean SST). Each 30-yr (1984–2014) annual value for JJASON is used. The vector of global mean SST is fixed, but a vector of TC climate varies by each angle. Finally, the correlation between TC climate and global ocean warmth is mapped with a loop on the correlation screen. Correlation shows the similarity of this environment with another synthetic environment brought about by global ocean warmth. The purple loop is the correlation using data from JTWC, and the green loop is the correlation using data from JMA. The thick orange and red loop is the correlation using composite data from the JTWC and JMA. The center, inner circle, and outer circle in gray (Fig. 2)

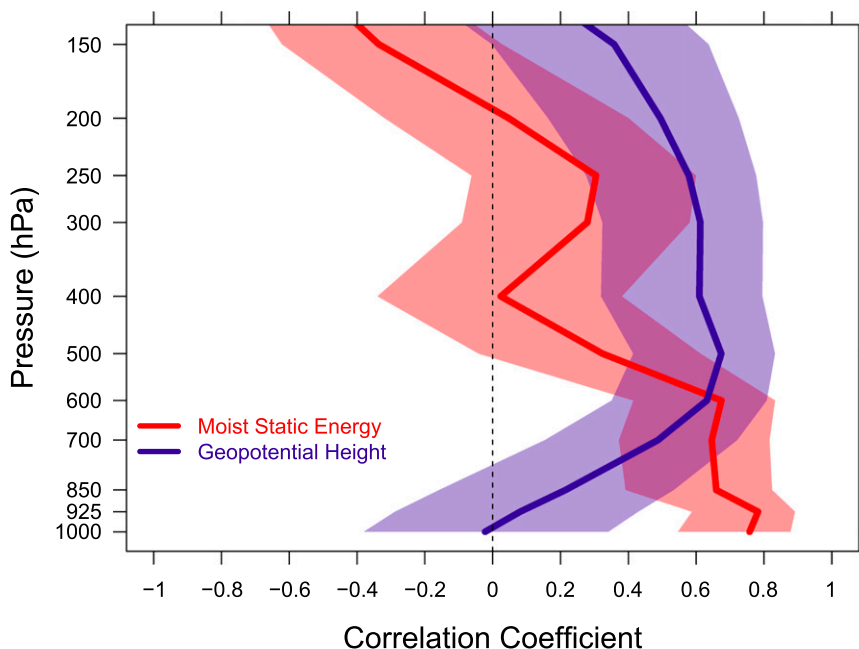


FIG. 3. Correlation profile of global ocean warmth with moist static energy and geopotential height in the tropical region (0° – 30° N) of the western North Pacific (100° E– 180°). The significant correlation range ($\alpha \leq 0.05$) at each pressure level is shaded. All values are averaged for JJASON over 30 years (1984–2013) to calculate correlations. The ENSO influence is removed separately from each variable, so the values represent the partial correlation. The graph shows the thermodynamics of a globally warm environment at the same ENSO condition.

indicate the correlation levels of 0, 0.5, and 1, respectively.

Principal component analysis is used to composite JTWC and JMA observations. **FRQ** and **INT** are the principal components, which indicates the in-phase relationship between the two observations. **FRQ** is represented as

$$\mathbf{FRQ} = [s(\mathbf{FRQ}_{\text{JTWC}}) + s(\mathbf{FRQ}_{\text{JMA}})]/\sqrt{2}, \quad (4)$$

where the operator $s()$ returns standardized values of an input vector as expressed in Eqs. (1) and (2). Likewise, **INT** is represented as

$$\mathbf{INT} = [s(\mathbf{INT}_{\text{JTWC}}) + s(\mathbf{INT}_{\text{JMA}})]/\sqrt{2}. \quad (5)$$

The highest correlation $\{r = +0.75; [0.53, 0.87], 95\%$ confidence interval (CI) $\}$ occurs in the **EINT** direction (red dot). The statistically significant correlation range is indicated in red. As defined, higher **INT** can occur in years with higher **EINT** and higher **ACT**, and lower **FRQ** in years with higher **EINT** and lower **ACT**. However, since **EINT** is orthogonal to **ACT**, it represents the out-of-phase relationship between **INT** and **FRQ**. Thus, the strong correlation along the **EINT** direction makes it clear that global ocean warmth

influences the collinearity between **INT** and **FRQ** rather than influencing **ACT** alone or either **INT** or **FRQ** individually.

4. TC environment

Increasing **EINT** (fewer TCs but stronger super-typoons) is an empirical result that arises from synchronous changes to physical factors under the influence of global warming (see Fig. 2). A decrease in **FRQ** together with an increase in **INT** results from an increase in saturation deficit occurring in the tropical free atmosphere in concert with a decrease in upward mass flux. Figure 3 shows that the climate dynamics for the global tropics explained by Kang and Elsner (2015) is also valid and even more apparent in the tropical region of the western North Pacific. Here, specific humidity and geopotential height as well as air temperature are used for the plot, with data coming from the NCEP re-analysis. To find a clear response of the regional environment to global ocean warmth, ENSO influence (indicated by a negative SOI value) is statistically removed from variables, and the partial correlation is calculated. Then we determine the western North Pacific TC environment at the same ENSO conditions

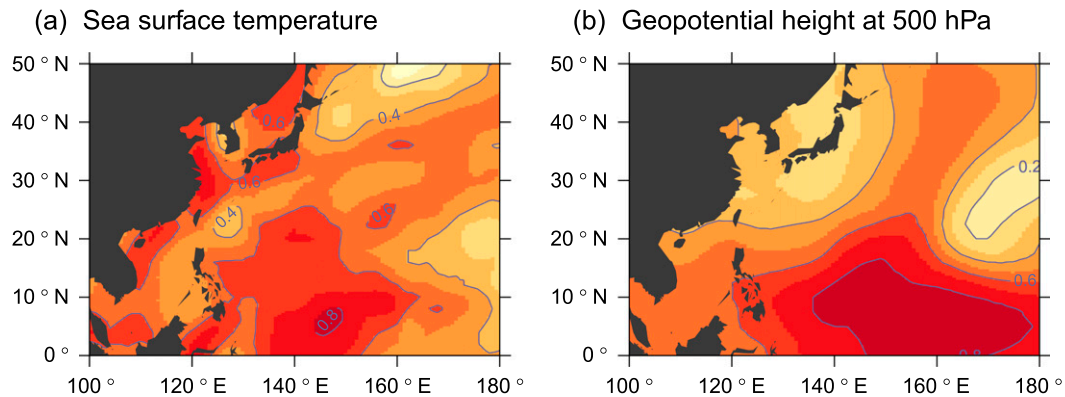


FIG. 4. Correlation maps of global ocean warmth with (a) regional SST and (b) regional geopotential height at 500 hPa. At each grid point, ENSO influence is removed from the variables, and partial correlation is calculated. Thus, the result shows the regional pattern of a globally warm environment at the same ENSO condition. Global mean SST is used as an indicator of global ocean warmth. All values are averaged for JJASON over 30 years (1984–2013) to calculate correlations.

(statistically) when global ocean warmth is increasing. In globally warm years, regional SSTs across the tropical western North Pacific are also above normal. The increase in regional SST itself is a positive environmental factor for **ACT**. As warmth increases, the lower troposphere in this region gains additional moisture following the Clausius–Clapeyron relationship. However, aloft in the free atmosphere the moisture gain is less (Held and Soden 2006). This is different from temperature changes in the middle and upper troposphere, which increase significantly by convection following a moist adiabat (Chou et al. 2013). Though the temperature is also influenced by dynamic and radiative processes, the major change is driven by the moist convection. The vertical profile of correlation confirms that moist static energy increases in the western North Pacific (0° – 30° N, 100° E– 180°) are more pronounced in the lower troposphere under increasing global temperature. This environmental change implies a convectively more unstable troposphere, which leads to more **ACT** (greater **FRQ** and **INT**).

In contrast, regionally increasing air pressure aloft (at a constant geopotential height) inhibits **ACT**. Unlike in the lower troposphere, where pressure is influenced by the air mass above, in the middle and upper troposphere pressure is directly influenced by air temperature. The vertical profiles of correlation show that geopotential height is strongly colinear with higher SST, implying a cap on the destabilized troposphere. Since temperature is well stratified, the air pressure anomaly over the middle and upper troposphere is also stratified, leading to a decrease in the upward mass flux (Sugi and Yoshimura 2012). If high pressure aloft is dominant, then convection has limited opportunity to transport energy from the lower troposphere, leading to fewer

TCs. Yet, considering the large moist static energy, the limited opportunity implies stronger TCs for those that do form (Kang and Elsner 2015). Therefore, as demonstrated by the large and significant correlation between western North Pacific **EINT** and global temperature, we can conclude that the convectively destabilized troposphere with large moist static energy in this region accompanied by a strong pressure anomaly aloft inhibits overall TC occurrences, but TCs that do form are likely to obtain greater intensity (on average) resulting from the discharge of additional energy.

Figure 4 shows correlation maps of global ocean warmth with regional SST and regional geopotential height at 500 hPa, where partial correlation is computed at each grid point. Compared with Fig. 5 where ENSO variation is not removed, the regional SST is seen to be even more pronounced. Enhanced regional SST anomalies accompanying the global ocean warmth variation provide a better understanding of the anomalous high.

5. Time series of global ocean warmth and 10% of the strongest typhoons

As **INT** is the combination of **ACT** and **EINT**, **EINT** implies the portion of **INT** that is not influenced by **ACT**. In other words, **EINT** represents the **INT** variation (the negative **FRQ** variation at the same time) where an internal variation (**ACT**) is removed. Trends and annual fluctuations over the 30-yr period (1984–2013) confirm a tight connection between global ocean warmth and **EINT** at this extreme portion (Fig. 6). The trend of standardized SST over the period is $+2.8 \pm 0.37$ standard deviations per 30 yr (where 0.37 is the standard error), which compares with the trend in **EINT** of $+2.0 \pm 0.52$ standard deviations per 30 yr. The correlation

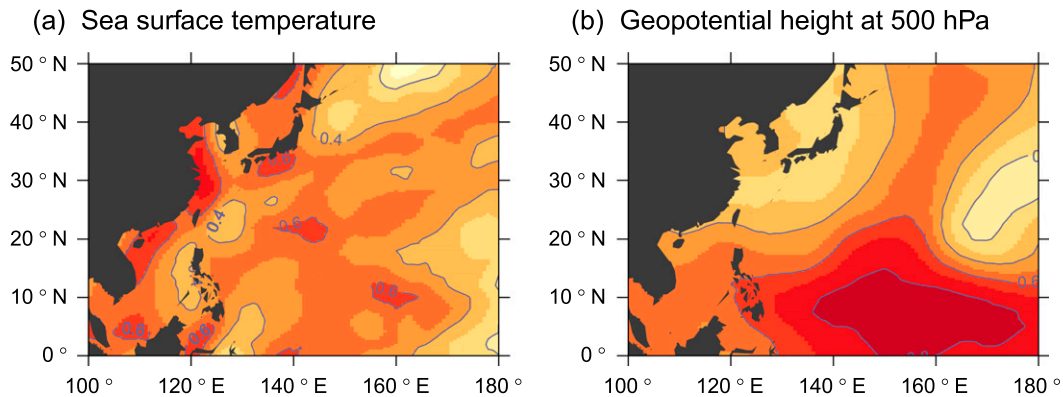


FIG. 5. As in Fig. 4, but using correlation rather than partial correlation. This is to see the influence of ENSO variation.

between the two series is $+0.75$ ($[0.53, 0.87]$, 95% CI) that reduces to $+0.57$ ($[0.25, 0.77]$, 95% CI) after removing the linear trends. The results clarify that supertyphoons are likely to become stronger at the expense of overall TC frequencies in a warmer world regardless of variations to **ACT**. The time series of global ocean warmth (red line) indicates how the TC environments have evolved to enhance the intensity of supertyphoons in the western North Pacific. Standardized **EINT** values are averaged to be -0.12 and 0.75 (standard deviation) for each of the last two decades, confirming the recent TC climate feature of lowering frequency but stronger intensity.

6. Summary and discussion

Among the TC climate variability directions, we find that **EINT** for 10% of the most intense TCs is strongly influenced by global ocean warmth. The thermodynamic structure of the tropical western North Pacific with high global ocean warmth is characterized by a convectively more unstable lower troposphere but a simultaneously prevailing high pressure anomaly in the middle and upper troposphere. Increasing **EINT** in a warmer year shows that this environment further inhibits the TC occurrences over the region, but TCs that form tend to discharge stored energy to the upper troposphere with stronger intensities. As the increasing intensities compensate for the loss of **ACT** by decreasing number of TCs, the **ACT** remains largely unchanged. As the strongest 10% of the TCs are on average comparable to supertyphoons, the increasing **EINT** suggests clearly that supertyphoons in warmer years get stronger. The study is unique in that it does not use smoothing or wavelet transforms. It explores directly the annual variation of TC climate with global SST, which is a useful indicator of global ocean warmth. Thus, it is not necessary to assume an increasing trend as the influence

of global warming. In contrast to the classical way of trend analysis, here global warming influences on the two best tracks in JJASON are compared to find a reliable TC climatology. In addition, this study clarifies the background thermodynamics by computing partial correlations on the environmental variables.

Assuming the warming trend in the oceans continues, this study implies we will likely experience a year warmer than ever and thus a larger **EINT**. By definition, a larger **EINT** means a larger gap between intensity and frequency, with the consequence of record strong supertyphoons at the expense of fewer overall TCs. Figure 7 summarizes the findings from a linear perspective. TC activity is demonstrated as a variation that is independent of global warming and can be assumed to be internal variability having no trend. Frequency variation and supertyphoon intensity variation are regarded as the addition of global warming influence on TC activity variation. The structure depicts how a previous intensity record is overtaken while frequency falls in our global warming environment. A year with record global ocean warmth is likely

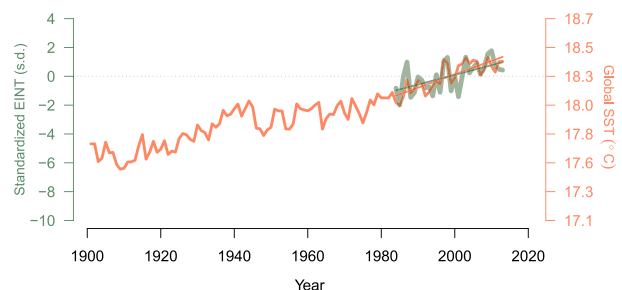


FIG. 6. Time series of global ocean warmth (red line) and **EINT** (green line) in the western North Pacific. Global mean SST is used to indicate global ocean warmth. Values are standardized to the 30-yr period (1984–2013) and the scale for SST values is presented on the right axis.

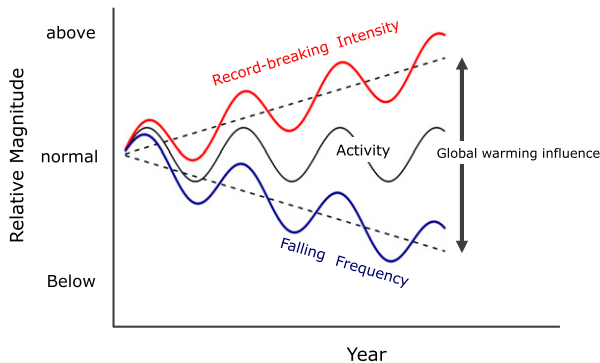


FIG. 7. Schematic of global warming's influence on TC climate in the western North Pacific. Intensity variation is the linear combination of activity and efficiency of intensity, while frequency variation is the linear combination of activity and negative efficiency of intensity. Global warming influences the efficiency of intensity rather than activity. From a linear perspective, this climate change results in record-breaking intensities with fewer tropical cyclones.

to experience a record-breaking intensity even during a lull in TC activity.

Acknowledgments. This work was supported by the National Typhoon Center at the Korea Meteorological Administration (“Development and Application of Technology for Weather Forecast” project) and the Geophysical Fluid Dynamics Institute at Florida State University.

REFERENCES

- Bell, G. D., and Coauthors, 2000: Climate assessment for 1999. *Bull. Amer. Meteor. Soc.*, **81** (6), s1–s50, doi:10.1175/1520-0477(2000)81[s1:CAF]2.0.CO;2.
- Chan, J. C. L., 2005: Interannual and interdecadal variations of tropical cyclone activity over the western North Pacific. *Meteor. Atmos. Phys.*, **89**, 143–152, doi:10.1007/s00703-005-0126-y.
- , 2006: Comment on “Changes in tropical cyclone number, duration, and intensity in a warming environment.” *Science*, **311**, 1713, doi:10.1126/science.1121522.
- , 2008: Decadal variations of intense typhoon occurrence in the western North Pacific. *Proc. Roy. Soc. London*, **A464**, 249–272, doi:10.1098/rspa.2007.0183.
- Chou, C., T. C. Wu, and P. H. Tan, 2013: Changes in gross moist stability in the tropics under global warming. *Climate Dyn.*, **41**, 2481–2496, doi:10.1007/s00382-013-1703-2.
- Elsner, J. B., J. P. Kossin, and T. H. Jagger, 2008: The increasing intensity of the strongest tropical cyclones. *Nature*, **455**, 92–95, doi:10.1038/nature07234.
- Emanuel, K. A., 2005: Increasing destructiveness of tropical cyclones over the past 30 years. *Nature*, **436**, 686–688, doi:10.1038/nature03906.
- , 2008: The hurricane–climate connection. *Bull. Amer. Meteor. Soc.*, **89**, ES10–ES20, doi:10.1175/BAMS-89-5-Emanuel.
- Held, I. M., and B. J. Soden, 2006: Robust responses of the hydrological cycle to global warming. *J. Climate*, **19**, 5686–5699, doi:10.1175/JCLI3990.1.
- IPCC, 2013: *Climate Change 2013: The Physical Science Basis*. Cambridge University Press, 1535 pp., doi:10.1017/CBO9781107415324.
- Kang, N.-Y., and J. B. Elsner, 2012a: An empirical framework for tropical cyclone climatology. *Climate Dyn.*, **39**, 669–680, doi:10.1007/s00382-011-1231-x.
- , and —, 2012b: Consensus on climate trends in western North Pacific tropical cyclones. *J. Climate*, **25**, 7564–7573, doi:10.1175/JCLI-D-11-00735.1.
- , and —, 2015: Trade-off between intensity and frequency of global tropical cyclones. *Nat. Climate Change*, **5**, 661–664, doi:10.1038/nclimate2646.
- Klotzbach, P. J., 2006: Trends in global tropical cyclone activity over the past twenty years (1986–2005). *Geophys. Res. Lett.*, **33**, L10805, doi:10.1029/2006GL025881.
- Knapp, K. R., and M. C. Kruk, 2010: Quantifying interagency differences in tropical cyclone best-track wind speed estimates. *Mon. Wea. Rev.*, **138**, 1459–1473, doi:10.1175/2009MWR3123.1.
- Knutson, T. R., and Coauthors, 2010: Tropical cyclones and climate change. *Nat. Geosci.*, **3**, 157–163, doi:10.1038/ngeo779.
- Kossin, J. P., T. L. Olander, and K. R. Knapp, 2013: Trend analysis with a new global record of tropical cyclone intensity. *J. Climate*, **26**, 9960–9976, doi:10.1175/JCLI-D-13-00262.1.
- NDRRMC, 2014: Updates re the effects of Typhoon “Yolanda” (Haiyan). [Available online at [http://www.ndrrmc.gov.ph/attachments/article/1329/Update_on_Effects_Typhoon_YOLANDA_\(Haiyan\)_17APR2014.pdf](http://www.ndrrmc.gov.ph/attachments/article/1329/Update_on_Effects_Typhoon_YOLANDA_(Haiyan)_17APR2014.pdf).]
- Simpson, R. H., 1974: The hurricane disaster—Potential scale. *Weatherwise*, **27**, 169–186, doi:10.1080/00431672.1974.9931702.
- Song, J. J., J. Wang, and L. Wu, 2010: Trend discrepancies among three best track data sets of western North Pacific tropical cyclones. *J. Geophys. Res.*, **115**, D12128, doi:10.1029/2009JD013058.
- Sugi, M., and J. Yoshimura, 2012: Decreasing trend of tropical cyclone frequency in 228-year high-resolution AGCM simulations. *Geophys. Res. Lett.*, **39**, L19805, doi:10.1029/2012GL053360.
- Webster, P. J., G. J. Holland, J. A. Curry, and H.-R. Chang, 2005: Changes in tropical cyclone number, duration, and intensity in a warming environment. *Science*, **309**, 1844–1846, doi:10.1126/science.1116448.